

Reliability Based Design Optimization of a Long-Range eVTOL Aircraft under Uncertain Mission Parameters

Damien M. Keijzer¹ and Saullo G. P. Castro¹

¹Delft University of Technology, University of Science

²Department of Aerospace Structures and Materials, Delft University of Technology

¹*damien.keijzer@gmail.com*

¹*S.G.P.Castro@tudelft.nl*

Abstract

The emerging market of Urban Air Mobility (UAM) introduces highly uncertain mission parameters due to the non-conformal aspects of the expected operation of Electrical Vertical Take-off and Landing (eVTOL) vehicles, Unmanned Traffic Management (UTM) and vertiport logistics. The present research proposes a methodology to quantify this operational uncertainty, while integrating it into the design of an eVTOL aircraft by means of a Reliability-based Design and Optimization (RBDO) approach. The baseline configuration is a long-range eVTOL named Wigeon, which was deterministically designed and optimized. The proposed stochastic-based MADO approach employs a Monte Carlo Simulation to estimate the energy requirements for a diverse range of mission parameters. The results indicate that the reliability driven method performs better at mitigating risk compared to the traditional method of using safety factors to create design margin. However, the RBDO method overall lacks a significant advantage over the deterministic optimisation due to the dominance of the cruising phase in the overall energy consumption. Leading, the lift-to-drag ratio to be the driving parameter to the overall energy efficiency. The study also highlights that the adoption of RBDO comes with added computational costs, and more sensitivity to local minima.

1 Introduction

The rise of Urban Air Mobility (UAM) is posing difficulties for traditional deterministic Multi-Disciplinary Analysis and Design Optimizations (MADO). UAM, a concept that gained traction from the 2010s onwards [6], differs radically from conventional air travel in terms of its market dynamics and operational characteristics. This disparity introduces a significant amount of uncertainty in its mission parameters. This presents a unique challenge for regular deterministic MADO as they often rely on semi-empirical methods in the preliminary design phases for sizing [15]. These methods tend to fall apart in such new and unlike fields due to their semi-empirical nature. Additionally, designers incorporate design margins to manage uncertainties and mitigate risks, leveraging insights from past experiences [11]. While this strategy enhances the design's conservatism, it could potentially result in an overdesigned airframe.

Examples of uncertainty sources within UAM are numerous, e.g vertiports require new types of air traffic management, such as unmanned traffic management (UTM), this can result in non-conformal approaches and loitering patterns [16]. Moreover, crucial mission parameters such as mission distance, transition height [14] and cruising altitude are also hard to predict due to either lack of regulations, dependency on the vertiport or simply lack of market knowledge [3].

The aim of this paper is to assess the sources of mission uncertainty for a long-range electric Vertical Takeoff and Landing (eVTOL) aircraft and incorporate them into a reliability-driven design optimisation. This approach is contrasted with a deterministic baseline design of an eVTOL. To achieve this objective, a recent design of a long-range eVTOL named the Wigeon is utilized [2].

Previous work on reliability based methods by [11], who compared a deterministic and reliability-based design optimisation (RBDO) framework for a general aviation aircraft powered by a fuel cell [11]. [4] investigated the

implementation of RBDO in the design of a firefighting airtanker [4]. More examples of applications can be seen in paper [10]. However, the previously mentioned papers had their reliability influenced by uncertainty in the performance properties of the aircraft e.g. the zero-lift drag and not by operational uncertainty.

In contrast, paper [5] designed a generic fighter considering mission uncertainties by means of a new methodology called effectiveness based design, which utilized the core trait of RBDO, imposing a required confidence level on the mission success rate and optimise the design accordingly. Limited research has been conducted concerning the application of stochastic methods within UAM however; the objective of this paper is to address this gap.

The paper is organized as follows. In section 2, the original Wigeon framework, the baseline, is presented. Subsequently, in subsection 2.2, the outline and quantification of sources of uncertainty are discussed. The subsequent section, subsection 2.3, introduces and explores the reliability-driven design. Moving forward to section 3, the results stemming from the various designs are introduced and their implications explored in section 4. Lastly, conclusions and recommendations are presented in section 5 and subsection 5.1, respectively.

2 Methods

2.1 Baseline: The Wigeon

The Wigeon was developed for the Design Synthesis Exercise of 2021 and is a tandem rotating wing configuration with 12 propellers. Its MADDO coupled as shown Figure 1.

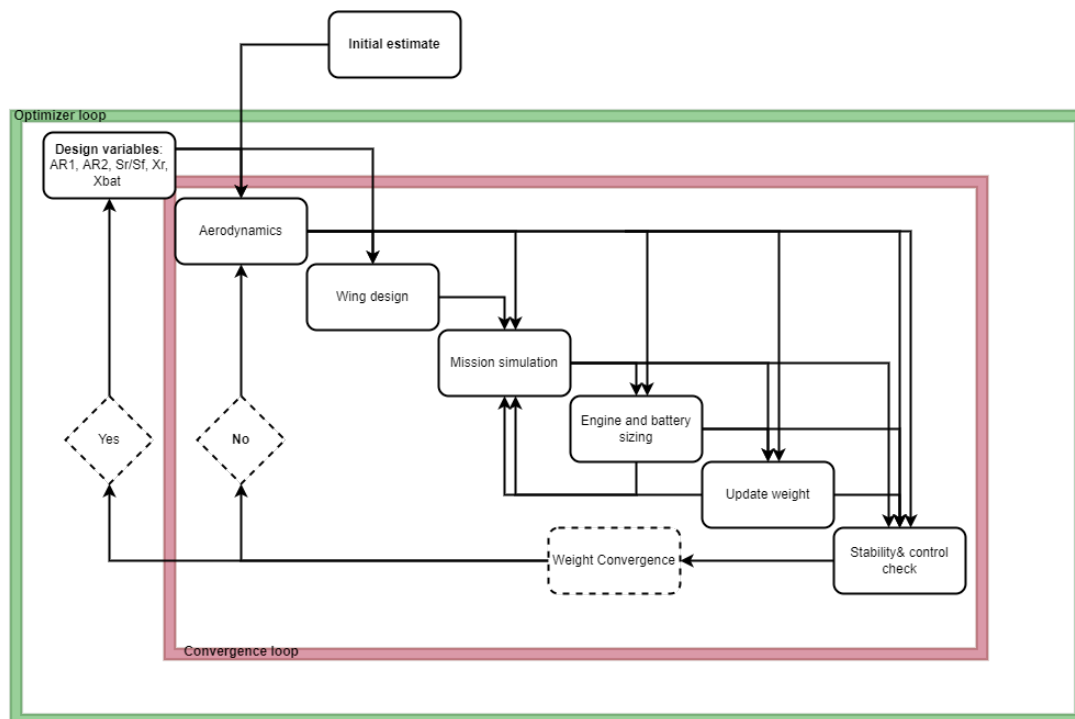


Figure 1: N2 chart illustrating the coupling of the MADDO used in the deterministic baseline version of the original Wigeon design.

The MADDO framework consists of a dual-loop structure. An inner convergence loop and an outer optimiser loop. The inner loop enforces the convergence of the design whenever alterations by the optimiser is made to the design. The outer loop changes the optimisation variables accordingly to the cost function at each outer loop. The MADDO framework encompasses three distinct types of variables; constants, internal variables and optimisation variables. constants require no further explanation. Internal variables refer to the parameters which dynamically adjust according to the optimisation variables. The internal variables require an initial estimate in order to start the MADDO procedure. Finally, the optimisation variables denote the parameters which are changed accordingly by the optimiser in order to minimize the objective function. In Table 1 a non-verbose tabular summary of the three different variables and what parameters they contain is shown.

Table 1: Non-verbose summary of the various variables involved in baseline MADO framework of the Wigeon.

Constants	Internal	Optimisation
Mission	MTOM	Aspect ratio's
Airfoil	Stall speed	Ratio surface area's
Taper	Wing mass	Position aft wing
Sweep	Battery mass	Battery position
Engines	wing geometry	

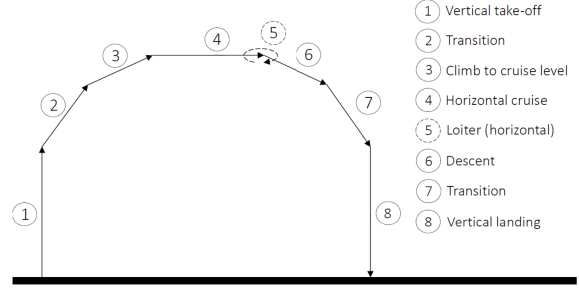


Figure 2: Mission profile used for mission performance analysis.

For an extensive explanation on all the disciplines and how they each size their respective subsystems please refer to [2]. However, the scope of this paper will limit itself to the mission simulation where the performance metrics are computed.

In the mission simulation the most crucial metrics are computed, the mission energy and power requirements. A fixed mission is used with a profile as shown in Figure 2. Two numerical simulation were made. The first is performed from take-off to the start of cruise and the second simulation concerns itself with the end of cruise until touchdown. Thus phases 1 to 3 and 6 to 8, respectively. The approach involves determining wing angle and thrust based on prescribed acceleration values, employing equations of motion in a vehicle-carried reference frame. The aerodynamic parameters are estimated using lifting line methods, considering lift curve, drag polar and fuselage geometry. A proportional controller aids in smooth transitions between ground, cruise, and descent, while ensuring safety close to the ground.

The majority of the energy is consumed in the cruising phase which is simply modeled through a constant speed and altitude. The brake power required is then computed through the lift over drag ratio and the propulsive efficiency.

The final phase to model is loitering in cruise configuration, i.e horizontal flight. This is performed at the optimal loiter speed at cruise altitude. Note that no loitering is performed in hover configuration. A complete description of the numerical simulation including equations can be found in [3].

The optimiser utilizes the energy consumption computed in the numerical simulation as its objective function. In the baseline version, the Constrained By Linear Approximation (COBYLA) optimiser is used [13]. Knowing this, a formal description of the MADO framework can be stated as in Figure 2.1.

$$\begin{aligned}
 & \min_{\mathbf{x}} E(\mathbf{x}) \\
 & \text{where } \mathbf{x} = [AR_1, AR_2, \frac{S_2}{S_1}, x_2, x_{bat}] \\
 & \text{with bounds } 5 \leq AR_1 \leq 15 \\
 & \quad 5 \leq AR_2 \leq 15 \\
 & \quad \frac{S_2}{S_1} \geq 0.01 \\
 & \quad x_2 \leq 8 \\
 & \quad 0.5 \leq x_{bat} \leq 2.5 \\
 & \text{subject to } Cm_\alpha \leq 0.12 \\
 & \quad MTOM \leq 3175 \\
 & \quad \Delta x_{ctrl} \leq -0.1 \\
 & \quad \frac{S_2}{S_1} \geq 0.01 \\
 & \quad 0.7 \leq \frac{b_2}{b_1} \leq 1.3 \\
 & \quad 7.4 \leq b_1 \leq 14 \\
 & \quad 7.4 \leq b_2 \leq 14
 \end{aligned} \tag{1}$$

Where subscript 1 and 2 indicate the front and rear wing, respectively. Let Δx_{ctrl} be the control margin, Cm_α the derivative of the moment coefficient with respect to the angle of attack, S the wing surface area, AR the aspect ratio and x the longitudinal position. The function $E(\mathbf{x})$ represents the energy consumption as a function of the design vector \mathbf{x}

The constraints and bounds set follow from either physical limitations or regulations imposed by regulatory bodies such as EASA [7]. For example the mass constraint follows from regulations whilst the span limit is a physical one to ensure the Wigeon is able to land on helipads.

Then using an initial estimate the MADO framework can be initiated until it has converged to a minimum.

2.2 Sources of Uncertainty

Before moving on to the reliability based adapted version, several sources of mission uncertainty have to be identified as to be used in the altered MADO. Based on the findings in the previous section several mission parameters have been identified which have a stochastic nature. The parameters chosen and their respective probability density functions (PDF) are described in the following sections. All PDF's are defined in SciPy [19] if any specific information is required. Note that loitering in hover configuration is an addition not included in the original performance simulation.

2.2.1 Range

In the analysis of range distribution, the emphasis is initially placed on flights within Europe, in alignment with the baseline report's indication that around 68.3% of aircraft operate in this region [1]. The Wigeon's projected urban usage and the need for new infrastructure further support this focus [1]. To facilitate plotting cities and their respective ranges, a design boundary of 400 km range is set, considering the potential for more range even though a mass contingency had been applied [2]. This approach is particularly relevant for wealthy, densely populated metropolitan areas, which are likely to invest in and witness frequent flights.

Obtaining this limit, a plot can be created of all the cities and their respective range as seen in Figure 3, the plot has been divided under four sub-figures depending on the GDP of the cities. This was done to avoid cluttering. The black circles represent cities which were isolated, i.e unreachable from any other given city due them laying outside of the 400 [km] range.

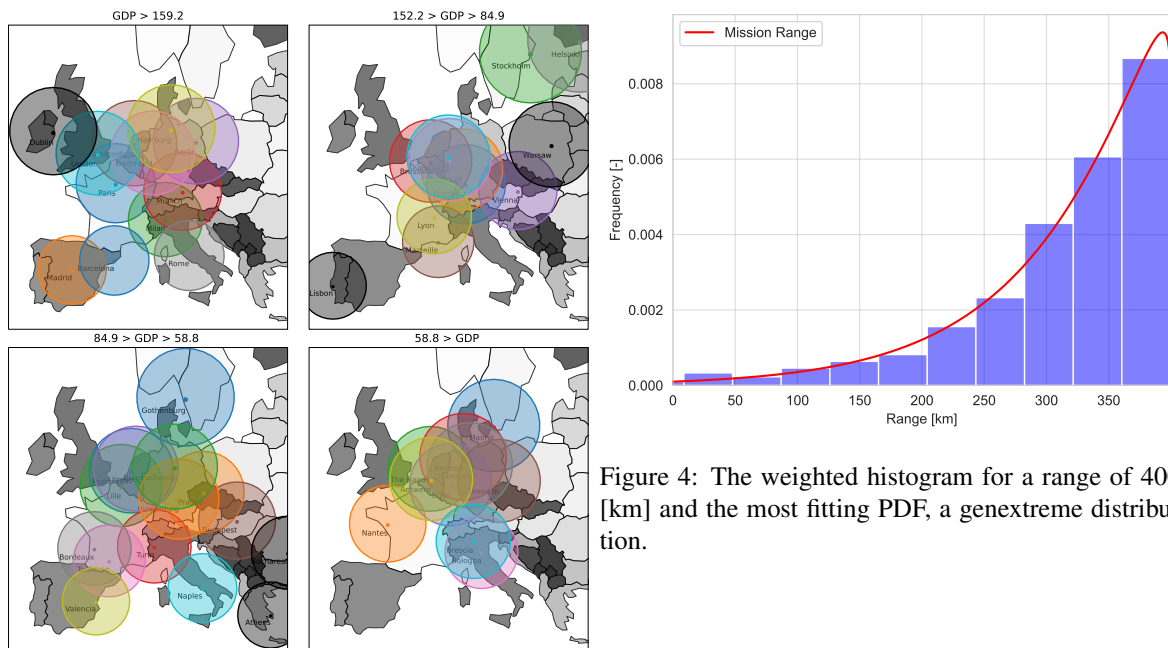


Figure 3: All 50 cities from [12] plotted with a surrounding circle of 400 [km]. A black circle indicating the corresponding city is isolated, meaning no connection to another city.

The isolated cities being Lisbon, Warsaw, Bucharest, Dublin and Athens. Looking at Figure 3, it is clear that most traffic will be concentrated in central Europe, meaning: France, Germany, Netherlands and England. Yet, there are some outliers in East and North of Europe but their access to other cities is limited and generally these cities are situated in the lower GDP range.

A key city in the analysis is London as it has the highest GDP, however it is only connected to central Europe through few cities in mainland Europe, a large proportion of the flights will occur between London and other major metropolitan areas, London-Dortmund et cetera. If only direct flights would have been allowed, this would

give a skewed representation of reality hence it was decided to allow one step in between. E.g London - Amsterdam - Dortmund. This will be referred to as a two-step flight.

Trip probabilities are systematically determined by enumerating feasible trips within the defined limit, forming the set Ω . For each trip, the GDP summation of departure and destination, e.g., [London-Paris] with GDP €1543.66 million (ζ_i), is calculated. Iterating over Ω yields a collection of ζ_i values, aggregating to total population GDP ζ_{tot} [Equation 2](#). Probability of a specific trip is $\frac{\zeta_i}{\zeta_{tot}}$ [Equation 3](#).

$$\zeta_{tot} = \sum_{i=0}^{\Omega} \zeta_i \quad (2) \quad P(T_i) = \frac{\zeta_i}{\zeta_{tot}} \quad (3)$$

The methodology is as follows. A histogram is made of all flights where the two-step flights have been split up into their child components. The bins of the obtained histogram are then scaled with their probabilistic expectation. As shown in [Equation 4](#), where f_{bin_i} represents the occurrence of the i_{th} bin, Ω_{bin} represents a sub-space of Ω containing all trips within the i_{th} bin. When child trips from the matching parent two-step flight occur in the same bin, the rule of addition and multiplication must be applied as shown in [Equation 5](#).

$$E[bin_i] = f_{bin_i} \cdot \sum_{j=0}^{\Omega_{bin}} P(T_j) \quad (4)$$

$$\begin{aligned} P(T_{i,1} + T_{i,2}) &= P(T_{i,1}) + P(T_{i,2}) - P(T_{i,1} \cap T_{i,2}) \\ &= P(T_{i,1}) + P(T_{i,2}) - P(T_{i,1}|T_{i,2}) \cdot P(T_{i,2}) \\ P(T_{i,1} + T_{i,2}) &= P(T_{i,1}) + P(T_{i,2}) - P(T_{i,2}) \\ P(T_{i,1} + T_{i,2}) &= P(T_{i,1}) = P(T_{i,2}) \end{aligned} \quad (5)$$

Where $T_{i,1}$ and $T_{i,2}$ represent the child trips of the two-step parent trips. The conditional probability $P(T_{i,1}|T_{i,2}) = 1$ in all cases since if one of the child trips occurs, the other by definition must then occur as well. The result from [Equation 5](#) then imposes alterations on [Equation 4](#) as shown in [Equation 6](#).

$$E[bin_i] = f_{bin_i} \cdot \left(\sum_{i=0}^{\Omega_{bin}} P(T_i) - \sum_{i=0}^{\Omega_{bin}} P(T_{i,2}) \text{if } (T_{i,2} \text{ and } T_{i,1}) \in \Omega_{bin} \text{ else } 0 \right) \quad (6)$$

The second summation sign corrects for the term $P(T_{i,1} \cap T_{i,2})$, an "if" and "and" statement are required since this only occurred when both child trips occurs in the space Ω_{bin} .

Performing the required analysis and computations then gives the results as shown in [Figure 4](#). A genextreme PDF, as described in [\[19\]](#).

2.2.2 Transition Height

As detailed in [\[3\]](#), the current simulation approach involves a sequence of actions. The aircraft begins by cruising at a designated altitude, followed by a controlled descent to the predetermined transition height. At this point, the aircraft initiates its transition to hover configuration, ensuring it remains above the Hover Hard Deck (HHD) altitude. Once the aircraft has completely reduced its horizontal speed, it gains the capability to descend below the HHD and proceed with the landing phase.

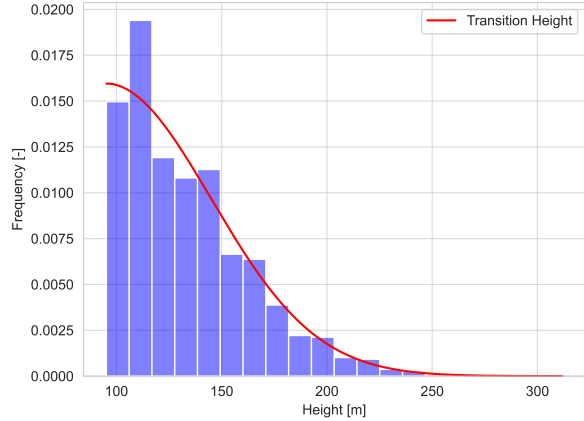
This scenario introduces two interrelated variables that require definition: the transition height (h_{trans}) and the Hover Hard Deck (HHD). These variables are closely linked, where raising the transition height would correspondingly raise the HHD.

Uber Elevate, set up vehicle and mission requirements for vehicles operating on their Elevate network [\[17\]](#). These requirements have been used in various studies from eVTOL to concept of operations (ConOps)[\[18\]](#).

The requirements are summarised in [Figure 5\(a\)](#). As can be seen from the table, Uber Elevate recommends to initiate transition, h_{trans} , at a height of 91 [m] (300 [ft]), and to have the HHD at 15 [m]. However, some papers

have diverged such as [14] which used 500 [m] for the h_{trans} . This however is relatively high when observing typical helicopter landings. The transition height will depend on the surrounding environment and airspace, in a metropolitan area like Frankfurt an increased h_{trans} will be required compared to e.g Amsterdam. Thus, the decision has been made to model the transition through a half-normal distribution as shown in Figure 5(b). Where the 91 [m] from Uber Elevate has been used a minimum.

Segment	Distance (mi)	Vertical Speed (ft/min)	Horizontal Speed (mph)	AGL Ending Altitude (ft)
A Ground Taxi	No Distance	0	3	0
B Hover Climb	Credit	0 to 500	0	50
C Transition + Climb	Sizing Repeated 60 25	500	0 to 1.2*Vstall	300
D Departure Terminal Procedures		0	1.2*Vstall	300
E Accel + Climb		500	1.2*Vstall to 150	1500
F Cruise		0	150	1500
G Decel + Descend		500	150 to 1.2*Vstall	300
H Arrival Terminal Procedures		500	1.2*Vstall	300
I Transition + Descend		500 to 300	1.2*Vstall to 0	50
J Hover Descend	No Distance	300 to 0	0	0
K Ground Taxi	Credit	0	3	0
L Reserves	Balked Landing, 6 mi divert at 500 feet AGL			



((a)) Summary of the mission requirements set by Uber Elevate[17]

((b)) The half-normal distribution for the transition height with a standard deviation of 50.

Figure 5

The final variable which has to be defined is the HDD. It will be defined as in Equation 7. The number 80 has been derived from the original height difference given by Figure 5(a) from Uber elevate. Thus, the assumptions is made that transition will always take place with a 80 [m] height difference.

$$h_{hhd} = h_{trans} - 80 \quad (7)$$

2.2.3 Loitering

The main purpose of loiter with respect to UAM, will be allowing the eVTOL to wait for a touch and lift-off (TLOF) area to become available. As, eVTOL batteries only carry limited energy, this waiting time has to be as minimized. This has sparked a great deal of research into Unmanned Aircraft System Traffic Management (UTM). Source [14], which simulated multiple algorithms to ensure enough spacing between incoming flights. Another paper investigated the use of holding circles and holding points to safely lead the incoming aircraft to the TLOF [16]. Finally, NASA performed a simulation of an entire network of vertiports in Houston, Texas with a demand model based on rush hours [9]. The most important factors influencing the simulation was the demand model, amount of VTOL, amount of TLOF and charging stations. Either of these factors could form a bottleneck and cause a consequential amount VTOL to loiter around the vertiport waiting for an available TLOF. Unfortunately, their model did not keep track of how long each VTOL was kept on hold. Even if this were the case, it would not necessarily represent reality as all factors are still highly fluctuable per city. To present these large spread and lack of knowledge an uniform distribution has been chosen between 0 and 600 seconds. As shown in Equation 8 where the symbol L is used for the loitering phase.

$$L_{cr} \sim U\{0, 600\} \quad (8)$$

The mission profile for the RBDO version will differ in cruising height for the loitering phase thus the mission profile shown in Figure 2 is altered. Reason being that that loitering will most likely take place in holding circles at a lower altitude according to [16] [16]. Whether, the aircraft will loiter pre - descent or in a holding circle post-descent will be dependent on the vertiport, airspace restrictions et cetera. The conservative decision has been made to only consider loitering post-descent. The loiter altitude should always be above the transition altitude. For simplification, Equation 9 will be used for the loiter altitude.

$$h_{loiter} = 1.2 \cdot h_{trans} \quad (9)$$

Finally, loitering in hover has to be considered, the assumption is made that only incidents will force the Wigeon to hover as it will mostly try to be avoided. This could for instance occur when an aircraft has to commit to an emergency landing when the Wigeon has just finished transition to prepare for landing. In this situation the energy state of the Wigeon would be too low to fly in cruise configuration thus it would have to hover to await a free TLOF.

The probability of this occurring is slim, therefore a Bernoulli distribution is chosen in combination with time it takes to descend to the TLOF. Reason being, that the Wigeon will only hover for the amount of time it takes to clear the TLOF. This can be computed using the descent rate and h_{trans} and a safety factor of 1.4 to account for any ground procedures. The final distribution is as shown in [Equation 10](#).

$$L_{hover} \sim 1.4 \cdot \frac{h_{trans}}{v_{descent}} \cdot Ber(0.01) \quad (10)$$

2.3 RBDO: The Wigeon

The MADDO framework detailed in [Figure 1](#) is altered to implement the mission uncertainty analysis. The former mission performance simulation has been replaced with a Monte Carlo simulation where a single mission simulation has been replaced with an array of missions created by sampling the random mission variables. The methodology of the simulation itself has only been altered such that it contains a probability of a loitering phase in hover configuration, unlike in the deterministic method.

The Monte Carlo Simulation's convergence is ensured by conducting a running variance analysis on the energy consumption samples obtained. A maximum permissible percentual difference between the latest and second-to-last sets of samples, as well as between the second-to-last and third-to-last sets, is applied as a criterion for convergence. This process helps determine when the simulation has reached a stable state.

From the resulting mission samples a PDF can be made of the energy consumption and other relevant performance parameters. The resulting PDF is utilized to impose a confidence interval, this confidence interval indicates the reliability with which the aircraft can successfully complete the sampled missions. The implication being that due to taking into account the mission uncertainty, design margins previously built in by safety factors can be removed. the recombination of the various random variables will result in a minority of missions limiting the performance of the aircraft through stringent requirements. Thus to avoid this, the confidence interval is applied. Leading to a possibly more balanced design.

The formal presentation of the altered MADDO framework implementing RBDO is then as shown in [subsection 2.3](#). The changes with respect to [Figure 2.1](#) being that the function $E(\mathbf{x}, \zeta)$ is also dependent on the random vector ζ . Let c_i be the the confidence interval, E_{c_i} the energy consumption for which the interval holds true. All other parameters have been previously defined.

$$\begin{aligned}
& \min_{\mathbf{x}} E(\mathbf{x}, \zeta) && \text{subject to } Cm_{\alpha} \leq 0.12 \\
& \text{where } \mathbf{x} = [AR_1, AR_2, \frac{S_2}{S_1}, x_2, x_{bat}] && Prob[E(\mathbf{x}, \zeta) \leq E_{c_i}] \geq c_i \\
& \zeta = [\sim R, \sim L_{cr}, \sim L_{hvr} \dots] && MTOM \leq 3175 \\
& \dots \sim h_{trans}, \sim h_{hhd}, \sim h_{ltr}] && \Delta x_{ctrl} \leq -0.1 \\
& \text{with bounds } 5 \leq AR_1 \leq 15 && 0.7 \leq \frac{b_2}{b_1} \leq 1.3 \\
& 5 \leq AR_2 \leq 15 && 7.4 \leq b_1 \leq 14 \\
& \frac{S_2}{S_1} \geq 0.01 && 7.4 \leq b_2 \leq 14 \\
& x_2 \leq 8 \\
& 0.5 \leq x_{bat} \leq 2.5
\end{aligned} \quad (11)$$

2.4 Comparative Assessment

The designs configurations shown in [Table 2](#) were used to compare the baseline Wigeon to the altered reliability-driven framework. The table limits itself to the most influential parameters to the design outcome. For a full description of the configuration please see [\[8\]](#) (request for access required as of March 15, 2024). Let N_{iter} be the amount of iterations the MADDO stays within the convergence loop, MCS target the maximum required percentual difference between the sets of samples set_n , set_{n-1} and set_{n-1} set_{n-2} . Finally let initial $AR_{1,2}$ be the initial aspect ratios of the front and aft wing, respectively. As seen in [Table 2](#), three deterministic designs and two reliability driven designs were made. Each design configuration purposely chosen shown to illustrate different phenomenon.

Table 2: The initiated MADDO design and their relevant initiation parameters. See source [\[8\]](#) for full description of starting conditions.

Label	D1	D2	D3	RBDO1	RBDO2
MADDO type	Dtr	Dtr	Dtr	RBDO	RBDO
N_{iter}	10	8	10	8	10
Initial $AR_{1,2}$	[8,9]	[7,7]	[10,12]	[7,7]	[10,13]
MCS target	-	-	-	0.45%	0.45%
c_i	-	-	-	90%	90%
Dtr Range [km]	400	400	375	-	-
Dtr Loiter [min]	10	10	8	-	-
Dtr Transition height [m]	180	180	150	-	-
Dtr cruising height [m]	1000	1000	1000	1000	1000
Mass contingency	False	False	10%	False	False

Table 3: Results from the various design following from the parameters as shown in [Table 2](#).

	D1	D2	D3	RBDO1	RBDO2
m [kg] ¹	2144.6	2173.1	2387.3	2058.0	2039.8
AR_1 [-]	10.4	10.0	9.3	10.9	10.1
AR_2 [-]	13.9	13.3	12.6	10.8	13.7
b_1 [m]	8.0	8.0	8.1	7.0	7.8
b_2 [m]	10.5	10.3	10.5	8.4	10.1
S_1 [m]	6.2	6.4	7.0	6.6	6.0
S_2 [m]	7.9	7.9	8.7	7.0	7.5
E [kWh]	168.9	175.0	178.6	161.1	154.9
$\frac{S_2}{S_1}$ [-]	1.27	1.23	1.24	1.06	1.24
x_{bat} [m]	2.5	2.5	2.5	2.5	2.4
x_2 [m]	8.0	8.0	8.0	8.0	7.3

Maximum take-off mass

It is important to note the subtle differences between the configurations. Let us first shortly discuss the deterministic designs. D1 and D2 had an identical set up in deterministic mission, however their initial estimate for the aspect ratio differed. D1 and D2 were used to compare the deterministic MADDO to the RBDO method without influence from the mass contingency, simplifying the interpretation of the driving parameters. In contrast, design D3 investigated a more realistic scenario where the deterministic design mitigates risk by applying a mass contingency. To this purpose the deterministic mission was altered, decreasing the range, loiter and transition height by minor increments. The risk of the deterministic design being an underestimation of the mission parameters, which was dealt through by the mass contingency.

On the contrary, the RBDO method encompasses a distribution of missions and a confidence interval to deal with the equivalent risk. Therefore, a mass contingency is not required. The reliability-driven design consists of two configurations with different initial aspect ratios to investigate local minima.

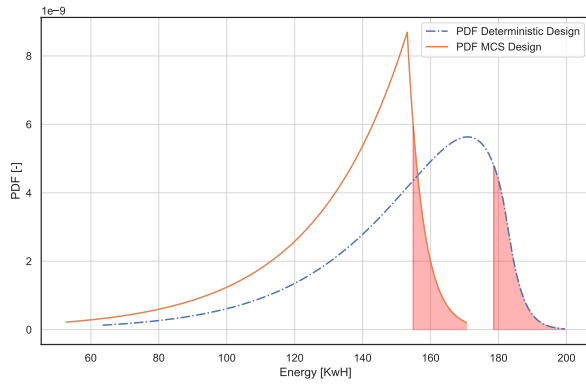
3 Results

The result of the different designs can be seen in [Table 3](#), all optimisation variables are shown and additionally other internal parameters deemed relevant. A discussion on the results of the designs will follow in [section 4](#).

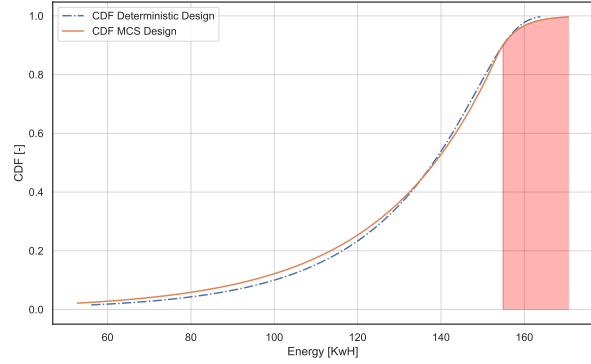
To observe the difference in performance between the RBDO and the baseline of the Wigeon, the baseline was subjected to a range of mission as defined by the random variables. Similar to the RBDO method, the resulting energy consumptions were collected and a PDF fitted. The resulting PDF and cumulative distribution function (CDF) are compared to the RBDO solution in [Figure 6\(c\)](#), [Figure 6\(b\)](#) and [Figure 6\(a\)](#). The red area under the graphs of the design of the RBDO method indicate the mission space which is excluded from the confidence interval.

The preceding plots provided a general overview of total energy consumption. To offer a more detailed breakdown, [Figure 6\(d\)](#) presents a pie chart illustrating energy consumption across different phases. Each pie's size reflects the 90th percentile, while the expectation and standard deviation for that phase are presented for reference.

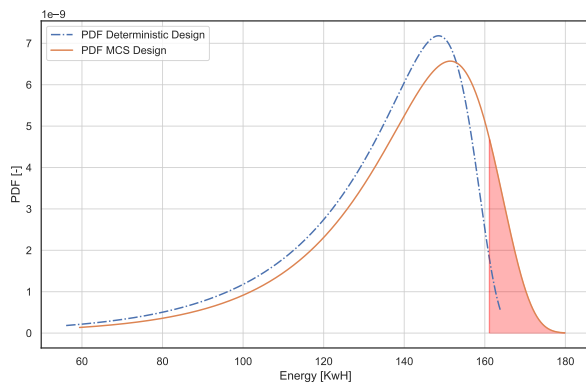
Additionally, to gain a better understanding of how the mission parameters influence the energy consumption the correlation coefficients of the resulting mission samples were computed and shown in [Table 4](#).



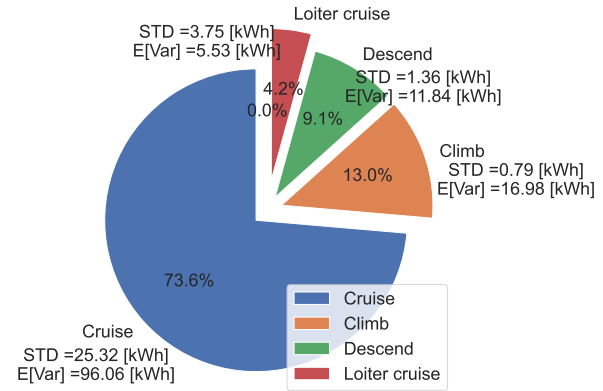
((a)) PDF of **D3** and **RBDO2** shown in blue and orange, respectively. The red area's indicate the mission space which is unavailable for the respective design.



((b)) PDF of **D1** and **RBDO2** shown in blue and orange, respectively. Red area being indicative for the mission space excluded by the confidence interval.



((c)) PDF of **D1** and **RBDO1** shown in blue and orange, respectively. Red area being indicative for the mission space excluded by the confidence interval.



((d)) Pie chart of design **RBDO2** of the various mission phases, the size of the pie dependent on the 90th percentile. The STD and expectation are listed in the vicinity

Figure 6: Visual illustrations of the performance of the various designs defined in [Table 2](#).

Table 4: The correlation coefficients between the mission energy random variable and the defining mission random variables.

	E	R	L_{cr}	h_{trans}	h_{ltr}	L_{hvr}
E	1	0.985	0.148	0.183	0.183	0.045

Finally, observing the weight distribution of the different designs gives insight into what trade-offs are being made. In accordance with this aim, a pie chart comparing design **RBDO1** and **D1** is shown in [Figure 7](#).

4 Discussion

The purpose of this paper was to investigate and quantify the mission uncertainty for a long-range urban Air Mobility (UAM) vehicle and implement them into an reliability-driven design optimisation. With the main goal of comparing its performance to a traditional deterministic multidisciplinary analysis & design optimization (MADO).

The differences between the deterministically designed aircraft and the reliability-driven design are minimal when comparing them without any mass contingencies. This is shown by [Figure 6\(b\)](#), here the performance of **D1** and **RBDO2** are compared through their respective CDF. The resulting CDF are nearly identical only having a slight difference due to the fact that **RBDO2** is subjected to less stringent mission requirements. This is indicated by

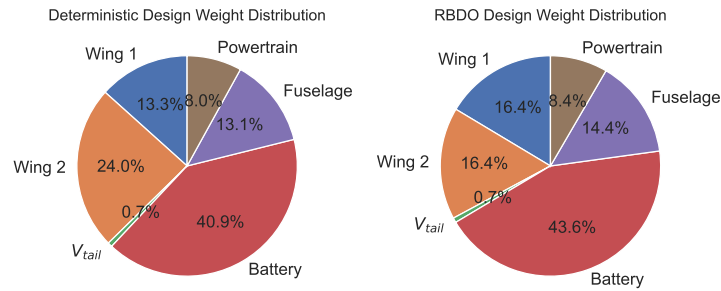


Figure 7: Pie charts of the weight distribution of design RBDO1 and D1

the red area, which marks the area of the top 10% most energy consuming missions not sized for. The maximum take-off mass advantage of design RBDO2 is portrayed by increased probability of flying missions with lower mission energies (and vice versa) as shown in Figure 6(b), where the CDF of RBDO2 remains above D1 until they intersect at roughly 135 [kWh].

Upon review of Figure 6(d), it becomes apparent why RBDO2 and D1 exhibit a strikingly similar design. The data depicted in Figure 6(d) highlights that, despite the irregular nature of missions in UAM, the cruising phase accounts for the majority of the energy consumption. Reason being that the Wigeon is a long-range UAM vehicle, therefore the cruising phase remains considerably long. The consequences of the dominating cruise phase being that the lift-over-drag becomes the driving parameter of the design, hence a nearly identical design with high aspect ratios and a significantly larger rear wing is preferred. This is further confirmed by Table 4, where the correlation coefficient for the random variable, $\sim R$, is extremely high almost reaching 1. Whilst the loitering in cruise configuration and transition height only show a weak positive correlation. Lastly, loitering in hover configuration gets completely diluted by the other dominant parameters. Based on these findings, the reliability driven method might be more suitable to short-range UAM vehicles.

When using mass contingencies however, a clear advantage can be seen. The result being as shown in Figure 6(a). The mass contingency snowballs the deterministic design into a much heavier design, severely effecting the performance. Whilst the contingency ensures the aircraft can still perform a majority of the missions while being affected by an underestimation of the mission parameters. The results suggest that it comes at a cost of moving away from the optimal design and an oversized battery. The proof being that the aspect ratio is noticeably smaller for D3, most likely to keep the structural weight down. Thus, overall adding design margin is not as suitable as a reliability-driven design is at mitigating risk. Nonetheless it is worth noting that while the current RBDO method tackles operational uncertainty, various of other sources of uncertainty are still present within the design e.g mass estimation methods. Therefore, completely removing the mass contingency from the RBDO method might have given a skewed interpretation of the results.

RBDO1 was the sole design to converge to a solution with relatively lower aspect ratios and equally sized wings. Suggesting it suffered from a local minimum it encountered starting from lower initial aspect ratios, the minimum caused by the fact that wings with higher aspect ratios are structurally heavier. This is illustrated by Figure 7, the rear wing for RBDO1 represents a lesser percentage than for D1. Notably, D2 does not suffer from this local minimum nearly as much even though starting from the same initial conditions. Nonetheless, it still ends up with slightly lower aspect ratios and a heavier design. Whilst not definitive proof, this is likely caused by the fact that a design with lower aspect ratios is not penalized as severely by the objective function in the RBDO framework. As the cases where lift-to-drag ratio is especially important, high range and long loitering, are excluded from the reliability-driven method. Thus, when the optimiser increases the aspect ratio, the structural weight increases, having a more negative effect on the overall distribution of missions. Resulting in the optimiser staying within this local minimum. All in all, the results demonstrate that the RBDO framework is more sensitive to local minima.

5 Conclusion

This study provided insights into the integration of mission uncertainty analysis using RBDO for long-range urban Air Mobility vehicles. While successful in demonstrating that the reliability driven design is more suitable for mitigating risk in contrast to using safety factors, the method's superiority over the deterministic MAD0 was

limited due to the energy intensive cruising phase. Leading the lift-over-drag ratio to be the driving parameter to be optimised for rather than a more moderate design with less structural weight for transition and hovering operations. Additionally, due to presence of uncertainty in areas other than its operation, safety factors might still be required or additional stochastic parameters added to the method. Finally, the reliability driven design also has additional sensitivity to local minima compared to the traditional deterministic method.

5.1 Recommendations

Several challenges were encountered when assessing the results, including computational power limitations and sensitivity to local minima. The computational power could be addressed by generating a more computational efficient numerical simulation. The potential for doing so being high, as it is currently implemented in Python, a notorious inefficient language. Regarding the sensitivity to local minima, an alternative optimisation technique could prove beneficial. An example being the genetic algorithm, which is useful at mitigating issues related to local minima. However, it's important to note that implementing this strategy might introduce additional computational overhead. Lastly, it is worth considering that the RBDO method might be better suited for UAM vehicles with shorter ranges, as they would experience a less dominant cruising phase. Exploring the application of this method to short range vehicles would provide valuable insights into its performance and effectiveness within a different mission domain.

References

- [1] Javier Alba-Maestre, Egon Beyne, Michael Buszek, Miguel Cuadrat-Grzybowski, Noah Salvador López, Nikita Poliakov, Koen Prud'homme van Reine, Alejandro Montoya Santamaría, Jakob Schoser, and Kaizad Wadia. Baseline Report - Multi-Disciplinary Design and Optimisation of a Long-Range eVTOL Aircraft, May 2021.
- [2] Egon Beyne, Michael Buszek, Miguel Cuadrat-Grzybowski, Noah Salvador López, Javier Alba-Maestre, Nikita Poliakov, Koen Prud'homme van Reine, Alejandro Montoya Santamaría, Jakob Schoser, and Kaizad Wadia. Final Report - Multi-Disciplinary Design and Optimisation of a Long-Range eVTOL Aircraft, October 2021.
- [3] Egon E. Beyne and Saullo G. Castro. *Preliminary performance assessment of a long-range eVTOL aircraft*.
- [4] Jr. Clark D.L., J.Y. Kao, C.H. Zeune, S.A. Burton, and E.E. Forster. Design of a conceptual firefighting airtanker vehicle using reliability-based design optimization. 2022.
- [5] D. L. Clark Jr., D.L. Allison, H. Bae, and E.E. Forster. Effectiveness-based design of an aircraft considering mission uncertainties. *Journal of Aircraft*, 56(5):1961 – 1972, 2019.
- [6] Adam P. Cohen, Susan A. Shaheen, and Emily M. Farrar. Urban air mobility: History, ecosystem, market potential, and challenges. *IEEE Transactions on Intelligent Transportation Systems*, 22(9):6074–6087, 2021.
- [7] EASA. Second publication of means of compliance with the special condition vtol. *MOC-2 SC-VTOL*, 3:49–62, 2022.
- [8] Keijzer, Damien and Beyne, Egon and Buszek, Michael and Cuadrat-Grzybowski, Miguel and López, Noah Salvador and Alba-Maestre, Javier and Poliakov, Nikita and Prud'homme van Reine, Koen and Santamaría, Alejandro Montoya and Schoser, Jakob and Wadia, Kaizad. RBDOWigeon. <https://github.com/dmkeijzer/RBDOWigeon.git>, 2023.
- [9] Lee W. Kohlman and Michael D. Patterson. *System-Level Urban Air Mobility Transportation Modeling and Determination of Energy-Related Constraints*.
- [10] Taewoo Nam and Dimitri Mavris. Multistage reliability-based design optimization and application to aircraft conceptual design. *Journal of Aircraft*, 55(5):2022 – 2036, 2018. Cited by: 5.
- [11] Taewoo Nam, Danielle Soban, and Dimitri Mavris. *A Non-Deterministic Aircraft Sizing Method under Probabilistic Design Constraints*.

- [12] Natural earth data. <https://www.naturalearthdata.com/downloads/10m-cultural-vectors/>. Accessed: April 25, 2023.
- [13] M. J. D. Powell. *A Direct Search Optimization Method That Models the Objective and Constraint Functions by Linear Interpolation*, pages 51–67. Springer Netherlands, Dordrecht, 1994.
- [14] Priyank Pradeep. *Arrival management for eVTOL aircraft in on-demand air mobility*. PhD thesis, 2019.
- [15] Daniel Raymer. *Aircraft design: A conceptual approach*, 1999.
- [16] Kyowon Song, Hwasoo Yeo, and Jung-Ho Moon. Approach control concepts and optimal vertiport airspace design for urban air mobility (uam) operation. *International Journal of Aeronautical and Space Sciences*, 22:1–13, 03 2021.
- [17] Uber. *Uber air vehicle requirements and missions*. Technical report, Uber, 2018.
- [18] Parker D. Vascik and R. John Hansman. *Development of Vertiport Capacity Envelopes and Analysis of Their Sensitivity to Topological and Operational Factors*.
- [19] Pauli Virtanen, Ralf Gommers, Travis E. Oliphant, Matt Haberland, Tyler Reddy, David Cournapeau, Evgeni Burovski, Pearu Peterson, Warren Weckesser, Jonathan Bright, Stéfan J. van der Walt, Matthew Brett, Joshua Wilson, K. Jarrod Millman, Nikolay Mayorov, Andrew R. J. Nelson, Eric Jones, Robert Kern, Eric Larson, C J Carey, İlhan Polat, Yu Feng, Eric W. Moore, Jake VanderPlas, Denis Laxalde, Josef Perktold, Robert Cimrman, Ian Henriksen, E. A. Quintero, Charles R. Harris, Anne M. Archibald, Antônio H. Ribeiro, Fabian Pedregosa, Paul van Mulbregt, and SciPy 1.0 Contributors. SciPy 1.0: Fundamental Algorithms for Scientific Computing in Python. *Nature Methods*, 17:261–272, 2020.